

# Sinomenine alleviates diabetic peripheral neuropathic pain through inhibition of the inositol-requiring enzyme 1 alpha-X-box binding protein 1 pathway by downregulating prostaglandin-endoperoxide synthase 2

Ji Chen<sup>1†</sup>, Peng Guo<sup>2†</sup>, Xinxin Liu<sup>2†</sup>, Huizhi Liao<sup>2†</sup>, Kemin Chen<sup>3</sup>, Yuxia Wang<sup>3</sup>, Jie Qin<sup>3</sup>, Fengrui Yang<sup>2,3\*</sup> 

<sup>1</sup>Department of Endocrinology, The First People's Hospital of Huaihua, Huaihua, China, <sup>2</sup>Department of Anesthesiology, The First People's Hospital of Huaihua, Huaihua, China, and <sup>3</sup>Department of Anesthesiology, Hengyang Medical School, The First Affiliated Hospital, University of South China, Hengyang, China

## Keywords

Diabetic peripheral neuropathic pain, Sinomenine, Spinal cord microglia

## \*Correspondence

Fengrui Yang  
Tel.: +86-166-7097-9693  
Fax: +86-745-2383694  
E-mail address:  
332530935@qq.com

*J Diabetes Investig* 2023; 14: 364–375

doi: 10.1111/jdi.13938

## ABSTRACT

**Introduction:** We tried to show the effect of sinomenine (SIN) in diabetic peripheral neuropathic pain (DPNP) and the related underlying mechanism.

**Methods:** Network pharmacological analysis and bioinformatics analysis were carried out for identification of the active ingredients of *Sinomenium acutum* and the related genes. The DPNP rat model was constructed and primary rat spinal cord microglial cells were isolated for *in vitro* cell experiments. The therapeutic role of SIN in DPNP was determined *in vivo* and *in vitro* through analysis of microglial cell activation and inflammatory response.

**Results:** Therapeutic role of *S. acutum* in DPNP was mainly achieved by regulating 14 key genes, among which the target gene prostaglandin-endoperoxide synthase 2 (*PTGS2*) of SIN might be the key gene. An *in vivo* experiment showed that SIN inactivated the inositol-requiring enzyme 1 alpha-X-box binding protein 1 pathway by downregulating *PTGS2*, which relieved pain symptoms in DPNP rats. It was confirmed *in vivo* that SIN inhibited the pathway through *PTGS2* to alleviate the activation of spinal cord microglial cells and inflammatory response.

**Conclusion:** SIN decreases the expression of *PTGS2* to inactivate the inositol-requiring enzyme 1 alpha-X-box binding protein 1 signaling pathway, which inhibits microglial activation, as well as the release of inflammatory factors, thus alleviating DPNP.

## INTRODUCTION

Diabetic peripheral neuropathic pain (DPNP) is a kind of pain directly resulting from the aberrant somatosensory system in diabetes patients in light of the International Association for the Study of Pain<sup>1</sup>. Inflammation plays an important role in the onset, as well as the maintenance, of DPNP<sup>2</sup>. Notably, inhibited generation and activation of microglial cells in the

dorsal spinal cord have been found to share an association with the neuropathic pain state, including that in DPNP<sup>3</sup>.

The *Sinomenium acutum* stem is a kind of popular traditional Chinese medicine applied for treatment of bone and joint diseases; sinomenine (SIN) is the only chemical marker in mainstream pharmacopeias that controls the quality of the *S. acutum* stem<sup>4</sup>. SIN plays an antinociceptive role in rats with neuropathic pain<sup>5</sup>. Treatment with SIN can partially inhibit prostaglandin-endoperoxide synthase 2 (*PTGS2*) expression to exert a protective function in inflammatory pain in a rat model<sup>6</sup>. The *PTGS2* inhibitor, meloxicam, can exert

†These three authors contributed equally to this work.

Received 14 June 2022; revised 12 October 2022; accepted 16 October 2022

antiallodynic effects on DPNP in a mouse model<sup>7</sup>. Of note, *PTGS2* can bind to endoplasmic reticulum stress sensor inositol-requiring enzyme 1 alpha (*IRE1α*) and thus activate its expression, resulting in *IRE1α* splicing of X-box binding protein 1 (*XBP1*) mRNA<sup>8</sup>. *IRE1α* and *XBP1s* are activated in neuropathic pain triggered by chronic constriction injury<sup>9</sup>. Notably, inhibition of *IRE1α*–*XBP1* ameliorates the progression of hyperalgesia induced by opioids<sup>10</sup>. Based on the aforementioned results, we proposed a hypothesis here that SIN might affect the development of DPNP by regulating the *PTGS2*-mediated *IRE1α*–*XBP1s* signaling pathway.

## MATERIALS AND METHODS

### Ethical approval

This experimental procedure and animal use protocol were approved by the Animal Ethics Committee of Affiliated Huaihua Hospital, Hengyang Medical School, University of South China, and the animal experiments followed the Animal Welfare Act and Public Health Service guidelines for the management and use of experimental animals specified by the National Institutes of Health.

### Network pharmacological analysis

The compound components of *S. acutum* were searched from the Traditional Chinese Medicine Systems Pharmacology Database and Analysis Platform database and screened with the condition of oral bioavailability  $\geq 30\%$  and drug likeness  $\geq 0.18$ <sup>11</sup>, and the corresponding targets were downloaded. Perl is a programming language suitable for writing simple scripts and complex applications. We used Strawberry Perl 5.30.1.1 combined with the UniProtKB search function in the UniProt database to correct the target name to the corresponding official gene symbol (limiting the species condition as “Homo sapiens”).

### Bioinformatics analysis

Human DPNP-related microarray GSE95849 was obtained through the Gene Expression Omnibus database. The microarray was equipped with the platform annotation file GPL22448, and contained six normal control samples and six DPNP samples (Table 1). The differential gene expression profiles were obtained using the R language “limma” package <https://bioconductor.org/packages/limma/>, with setting of  $\log_{2}FC > 1$ ,

and  $P < 0.05$  reviewed as the screening criteria of differential genes. The Pearson correlation coefficient of gene expression profiles in microarray GSE95849 was calculated by R language, setting  $P < 0.05$  as the screening criteria for obtaining differential genes of the relevant gene.

### Venn map delineation online

Through the Xiantao Scholar website (<https://www.xiantao.love/>), the target genes of active ingredients of *S. acutum* were intersected with differentially expressed genes from the Gene Expression Omnibus microarray data to obtain candidate genes.

### Pharmacological network visualization and protein–protein interaction network construction

Cytoscape software (Free Software Foundation, Boston, MA, USA) was used to draw the network relationship diagram of 14 candidate genes and their corresponding components of *S. acutum* components. Through the database STRING, the interaction of candidate genes was analyzed, where the species condition was limited to “Homo sapiens”. Cytoscape software was applied to construct a regulatory relationship network, with the degree and combine score values represented by circle size and color, and the top 10 key genes were selected according to the degree value.

### ClusterProfiler enrichment analysis

Using the R language “ClusterProfiler” package, the gene ontology and Kyoto Encyclopedia of Genes and Genomes functional enrichment analyses of 14 key genes were carried out, including biological processes, cellular components, molecular function and signaling pathways. The color of the dot showed the  $P$ -value, and the dot size showed the number of targets enriched.

### DPNP rat model construction and blood glucose monitoring

A total of 75 male Sprague–Dawley rats aged 6–8 weeks (150–200 g; Vital River, Beijing, China) were selected.

Rats were randomly used as control rats, or subjected to model establishment without further treatment (DPNP rats) or further treated with SIN (intraperitoneal injection of SIN), SIN + overexpression (oe)-negative control (NC; intraperitoneal injection of SIN and tail vein injection of NC of overexpression lentivirus), SIN + oe-*PTGS2* (intraperitoneal injection of SIN and tail vein injection of *PTGS2* overexpression lentivirus), SIN + oe-*PTGS2* + MKC8866 (intraperitoneal injection of SIN, tail vein injection of *PTGS2* overexpression lentivirus and oral administration of MKC8866), with 12 rats in each group. DPNP rats received intraperitoneal injection of 50 mg/kg of streptozotocin (STZ; S0130; Sigma-Aldrich, St. Louis, MO, USA) to induce diabetes. A total of 12 rats in the control group were injected with the same dose of normal saline. One week after STZ injection, blood was drawn from the rat orbit, and fasting blood glucose level was measured using a glucose meter (OneTouch Ultra Mini; Johnson & Johnson, New Brunswick,

**Table 1** | Clinical and demographic characteristics of the participants from microarray dataset

	Normal control	DPN
<i>n</i>	6	6
Sex	Female	Female
Age (years)	51.17 ± 6.08	57.33 ± 7.92
Fasting glucose (mmol/L)	5.10 ± 0.21	9.95 ± 2.11*

\* $P < 0.05$  versus normal control. DPN, diabetic peripheral neuropathy.

NJ, USA). The rats with blood glucose levels >250 mg/dL were considered to have diabetes, and rats with increased behavioral sensitivity to pain were identified as successful DPNP model rats. The success rate of DPNP modeling was 95%, and the successfully modeled rats were randomly divided into five groups.

All DPNP rats were administered since successfully modeled, namely, on the first day of the second week after STZ injection. SIN ([+]-4-hydroxy-3,7-dimethoxy-17-methylmorphin-7-en-6-one) was purchased from Aladdin (115-53-7; Shanghai, China) and dissolved in 0.9% normal saline. The drug was administered intraperitoneally daily at a dose of 1 mL/kg on the first day of successful DPNP model construction, namely, on the first day of the second week after STZ injection<sup>5</sup>. Behavioral sensitivity testing was carried out 3 h after each administration of SIN.

Next, 10  $\mu$ L lentivirus was injected into the tail vein of STZ rats on the first day of the successful DPNP model construction. The viral titer of lentivirus was  $5 \times 10^8$  TU. Meanwhile, 300 mg/kg MKC8866 (HY-104040; MedChemExpress, Monmouth Junction, NJ, USA) was orally administered every other day. MKC8866 was an inhibitor of the IRE1 $\alpha$ -XBP1s pathway<sup>12</sup>. Rats were killed under anesthesia with 1% pentobarbital sodium 4 weeks after STZ injection. The spine of the rat was dissected, and the L4–L6 segment of the spine was obtained from the rat and the nucleus pulposus tissue was isolated for subsequent experiments. Blood glucose levels and bodyweight of the rats were determined before they were killed. A schematic diagram for model establishment, treatment and sampling is shown in Figure 1.

### Neural pain behavioral test

Mechanical allodynia and thermal hyperalgesia were assayed for evaluating the response of rats to neural pain, as previously described<sup>13</sup>. During the test, pain hypersensitivity thresholds were tested using an electronic mechanical pain gauge (BME-404; Boerni, Tianjin, China) and a 50% mechanical paw withdrawal threshold (PWT) was recorded. In addition, an automatic pain stimulator (BME-410C; Boerni, Tianjin, China) was

used with the paw withdrawal latency (PWL) recorded. Behavioral analysis was processed in a quiet room between 09.00 and 12.00 hours.

### Primary microglial cell extraction and culture

Rats were euthanized. The spinal cord tissue was extracted from the L4 to L6 segment of the spine, immersed in 4 mL pre-cooled Hank's solution (H1387; Sigma, Shanghai, China) containing 15 mmol/L HEPES (Gibco, Carlsbad, CA, USA) and 0.5% glucose (Sigma-Aldrich), ground and filtered. Cells were collected by centrifugation at 400 g for 10 min. Cell supernatants were collected and subjected to gradient-density centrifugation using Percoll (P4937; Sigma, Shanghai, China), followed by collection of cells at the junction of the 50%/75% Percoll interface. Expression of the microglial cell marker OX42 was measured by immunofluorescence to identify the purity of microglial cells. The collected cells were rinsed with pre-cooled phosphate-buffered saline, and then resuspended in Dulbecco's modified Eagle's medium supplemented with 1% bovine serum albumin (11965092; Gibco, Grand Island, NY, USA), 10% fetal bovine serum (10099141; Gibco) and 1% penicillin/streptomycin (15070063; Thermo Fisher Scientific Inc., Waltham, MA, USA) for the subsequent experiments.

Microglial cells were seeded in six-well plates routinely cultured for 24 h to induce inflammation. Some cells without any treatment were used as controls, and the others were supplemented with 25 mmol/L glucose (G8270; Sigma) for a 24-h intervention. High glucose (HG)-stimulated cells were treated with SIN (12  $\mu$ mol/L SIN for a 24-h intervention), with SIN and further infected with oe-NC or oe-PTGS2 lentivirus for 48 h, or with SIN + oe-PTGS2 (for 48 h) + 0.3  $\mu$ mol/L MKC8866 (an IRE1 $\alpha$ -XBP1s pathway inhibitor; for 24 h). All the lentiviruses were purchased from Genechem (Shanghai, China).

### Enzyme-linked immunosorbent assay

Expression of PTGS2, IER1 $\alpha$ , XBP1s, tumor necrosis factor (TNF)- $\alpha$ , interleukin (IL)-1 $\beta$  and IL-6 in rat spinal cords and microglial cell supernatants was determined using the enzyme-

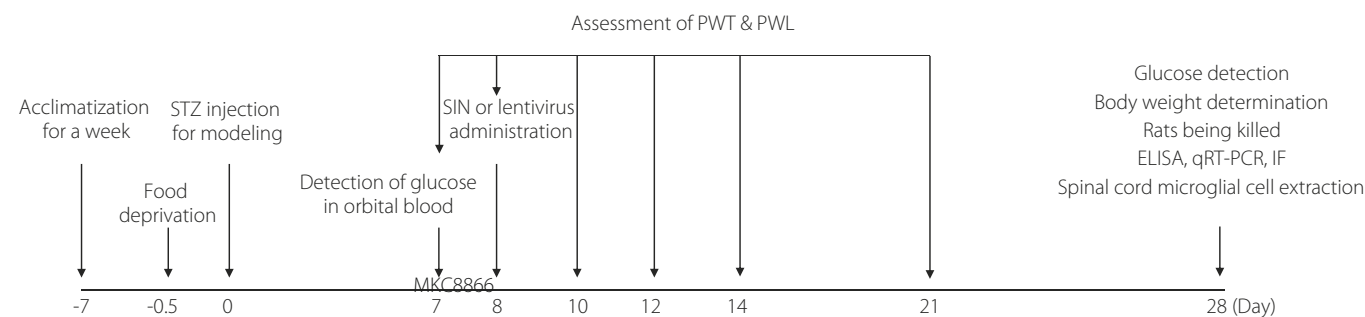


**Figure 1** | Schematic diagram of time points in the animal experiment. ELISA, enzyme-linked immunosorbent assay; IF, immunofluorescence; PWT, paw withdrawal latency; PWL, paw withdrawal threshold; qRT-PCR, reverse transcription quantitative polymerase chain reaction; SIN, sinomenine; STZ, streptozotocin.

linked immunosorbent assay (ELISA) kit: rat *PTGS2* (125–8,000 pg/mL, EKE62250; Biomatik, Wilmington, DE, USA), rat *IER1 $\alpha$*  (46.9–3,000 pg/mL, EKF59786; Biomatik), rat *XBP1s* (156–10,000 pg/mL, EKN49348; Biomatik), rat *TNF- $\alpha$*  (78.13–5,000 pg/mL, EKE61994; Biomatik), rat *IL-1 $\beta$*  (31.25–2000 pg/mL, EKE61988; Biomatik) and rat *IL-6* (62.5–4,000 pg/mL, EKE61991; Biomatik).

### Immunofluorescence

Paraffin sections of the L4–L6 segment of the spine were subjected to antigen retrieval. Next, the sections were immunostained with mouse anti-Ox42 (ab1211, 10  $\mu$ g/mL; Abcam Inc., Cambridge, MA, USA), mouse anti-neuronal nuclear antigen (NeuN; ab104224, 1:1000; Abcam), rabbit anti-NeuN (ab177487, 1:100; Abcam), rat anti-gial fibrillary acidic protein (GFAP; ab4648, 1:50; Abcam), rabbit anti-GFAP (ab7260, 1:50) and rabbit anti-*PTGS2* (ab179800, 1:50; Abcam) at 4°C overnight, as well as fluorescent secondary antibodies including goat anti-mouse (ab150115, 1:500; Abcam Inc.) and goat anti-rabbit (ab150077, 1:500; Abcam Inc.) at room temperature for 60 min. An Olympus BX51 fluorescence microscope (Olympus, Tokyo, Japan) or laser scanning confocal microscope (FV500; Olympus) was used to blindly observe all the sections, followed by photographing. Analysis was carried out using the Image Pro-Plus program and fluorescence intensity was recorded.

For cell samples, when spinal cord microglia reached 40–50%, they were fixed with 1 mL of precooled 95% ethanol for 30 min at  $-20^{\circ}\text{C}$ . The ethanol was discarded, and the cells were incubated with 5% bovine serum albumin at room temperature for 60 min. Excess serum was discarded and the cells were incubated with the corresponding primary antibody. The subsequent operations were as same as the tissue samples.

### Reverse transcription quantitative polymerase chain reaction

Total ribonucleic acid (RNA) was extracted from cells and frozen tissue samples using TRIZOL reagent (15596-018; Solarbio, Beijing, China). Total RNA was reversely transcribed into complementary deoxyribonucleic acid using the PrimeScript™ reverse transcription polymerase chain reaction kit (Takara, Dalian, China). Quantitative polymerase chain reaction was carried out on a LightCycler 480 system (Roche Diagnostics GmbH, Mannheim, Germany) using the SYBR Premix Ex Taq™ (Takara Biotechnology Ltd., Dalian, China).

Glyceraldehyde-phosphate dehydrogenase was used as an internal reference to standardize the messenger RNA expression. The primers were designed and synthesized by Anhui General Biotechnology Co., Ltd (Anhui, China). Primer sequences for *PTGS2* were forward: 5'-GTGGAAAAGCCTCGTCCAGA-3' and reverse: 5'-TCCTCCGAAGGTGCTAGGTT-3'; for glyceraldehyde-phosphate dehydrogenase were forward: 5'-AGACAGCCGCATCTTCTTGT-3' and reverse: 5'-TACGGCCAAATCCGTTTACA-3'. The relative quantitative method ( $2^{-\Delta\Delta C_T}$  method) was used to calculate the relative transcript level of the target gene.

### Statistical analysis

SPSS 21.0 (IBM Corp., Armonk, NY, USA) was applied to analyze data. Measurement data from three independent experiments were expressed as the mean  $\pm$  standard deviation. Comparisons on data between two groups were carried out using the independent samples *t*-test. Data comparisons among multiple groups were carried out by one-way analysis of variance (ANOVA). Comparisons on data between two groups that obeyed normal distribution were carried out using *t*-tests.  $P < 0.05$  showed statistical significance.

## RESULTS

### Network pharmacological analysis screened 115 effective target genes of *S. acutum*

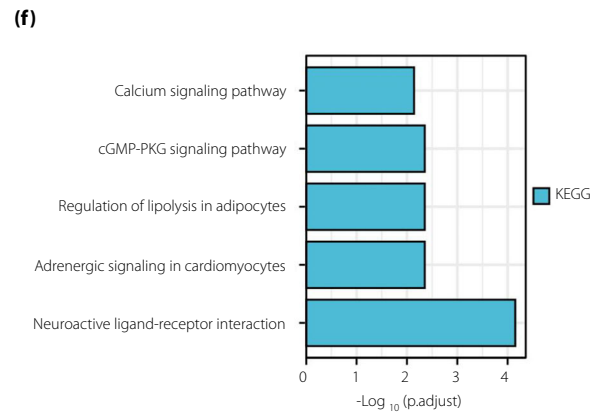
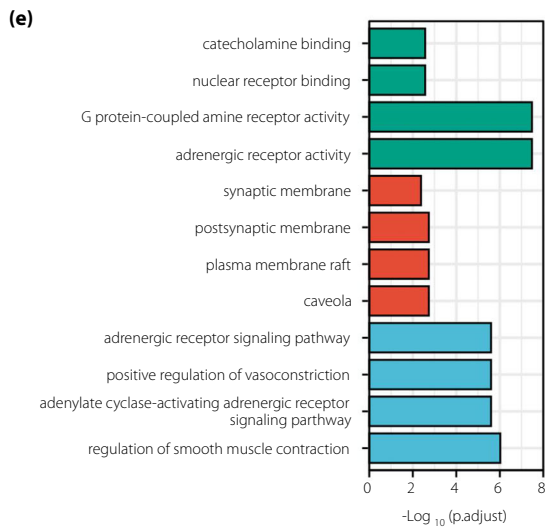
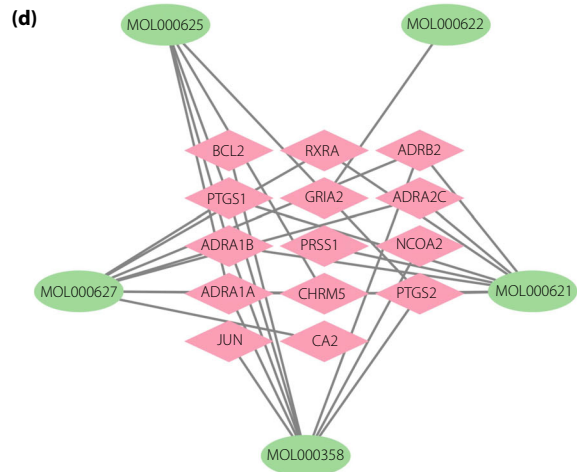
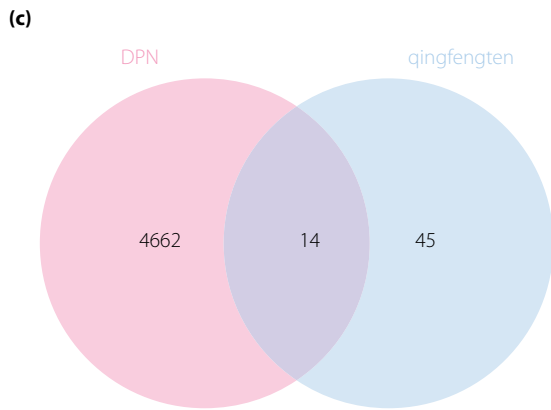
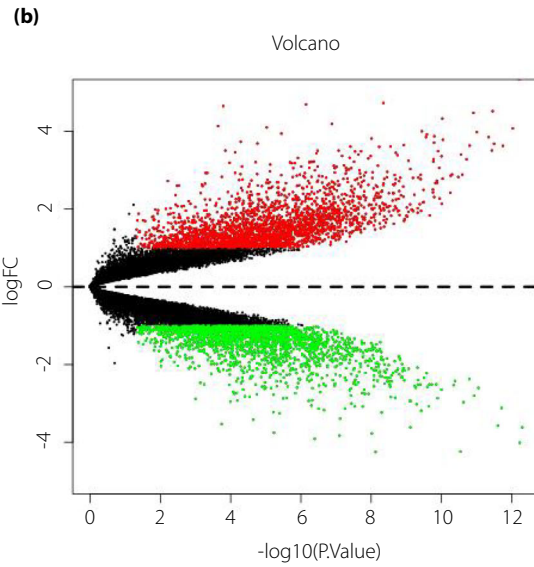
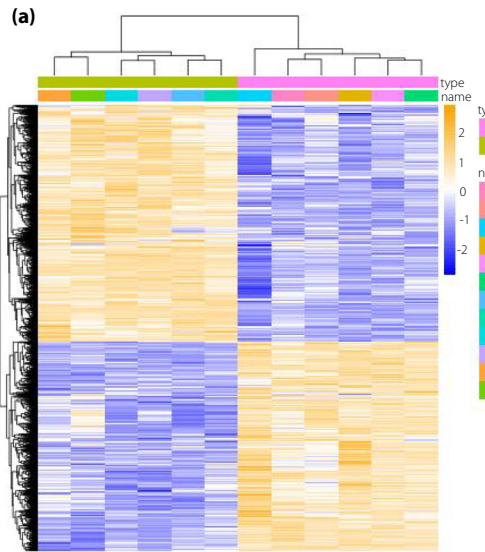
Six active ingredients (Table S1) were obtained after screening<sup>14</sup>, including MOL000358:  $\beta$ -sitosterol, MOL000621: 16-epi-isositsirikine, MOL000622: magnograndiolide, MOL000623: michelenolide, MOL000625: SIN and MOL00027: stepholidine.

As shown in Table S2, a total of 115 target proteins were obtained. Furthermore, the target proteins were converted into target genes through Perl language. As shown in Table S3, there were 38 target genes of  $\beta$ -sitosterol, 28 target genes of 16-epi-isositsirikine, four target genes of magnograndiolide, one target gene of michelenolide, 15 target genes of SIN and 29 target genes of stephanine.

### A total of 14 differential genes that *S. acutum* might act on to treat DPN were screened

The microarray GSE95849 was finally obtained, which contained 6 control samples and 6 DPNP samples. Analysis of the GSE95849 microarray dataset identified 4,676 differential genes,

**Figure 2** | A total of 14 differential genes that *Sinomenium acutum* might act on to treat diabetic peripheral neuropathy (DPN) are screened. (a) Heat map of the differential genes in the GSE95849 microarray (C represents control group [ $n = 6$ ], and T represents diabetic peripheral neuropathic pain [DPNP] group [ $n = 6$ ]). Blue indicates down-regulation and yellow indicates upregulation. (b) Volcanic map of the differential genes in the GSE95849 microarray ( $n = 6$  for the control and DPNP groups, respectively). Black dots represent genes that are not differentially expressed, red dots represent the upregulated genes and green dots represent downregulated genes. (c) Venn diagram for the intersection of differential genes in GSE95849 microarray and effective target genes obtained from network pharmacological analysis (the bar chart below shows the number of differential genes in DPNP and *S. acutum*). (d) Network diagram of “*Sinomenium acutum*-ingredients-target” (green circles represent the active ingredients of *S. acutum* and red diamonds represent the target genes which the active ingredients act on). (e) Bar chart of gene ontology function analysis of the 14 candidate genes at the biological process (BP), cellular component (CC) and molecular function (MF) levels. (f) Bar chart of the Kyoto Encyclopedia of Genes and Genomes (KEGG) pathway enrichment analysis of the 14 candidate genes.



including 2,195 downregulated genes and 2,481 upregulated genes (Figure 2a,b).

Differential genes in GSE95849 microarray dataset were intersected with target genes of active ingredients of *S. acutum* obtained from the Traditional Chinese Medicine Systems Pharmacology Database and Analysis Platform database. The results showed that 59 genes were left after the intersection. There were 14 intersection genes between Gene Expression Omnibus and target genes of active ingredients of *S. acutum* (Figure 2c, Table S4), which were *RXRA*, *ADRB2*, *ADRA2C*, *BCL2*, *ADRA1B*, *PRSS1*, *PTGS1*, *PTGS2*, *ADRA1A*, *CHRM5*, *GRIA2*, *NCOA2*, *CA2* and *JUN*. Five of them (*PTGS1*, *CHRM5*, *PTGS2*, *ADRA1A* and *ADRA1B*) were target genes of SIN.

Cytoscape software (Figure 2d) showed that the main active ingredients of *S. acutum* in DPNP were MOL000621: 16-epi-sisitsirikine, MOL000622: magnogradiolide, MOL000625: SIN, MOL000627: stephanine and MOL000358:  $\beta$ -sitosterol, corresponding to eight, one, five, eight and four target genes, respectively.

Furthermore, gene ontology and Kyoto Encyclopedia of Genes and Genomes function enrichment analyses of 14 key genes were carried out, the results (Figure 2e,f) showed that candidate genes were mainly involved in the main biological processes, including vascular smooth muscle contraction, adrenergic receptor signaling pathway and adenylate cyclase activation adrenergic receptor signaling pathway. The main cell components included synaptic membrane and postsynaptic membrane. The main molecular functions included G protein coupled amine receptor activity, adrenergic receptor activity, nuclear receptor binding and catecholamine binding. Neuroactive ligand receptor interaction was the main Kyoto Encyclopedia of Genes and Genomes pathway enriched. It has been documented that neuroactive ligand receptor interactions are associated with neuroprotection and inflammatory responses<sup>15,16</sup>. In addition, adrenergic signaling pathway in cardiomyocytes, regulation of adipocyte lipolysis and CGMP-PKG signaling pathway have been reported to be closely related to endoplasmic reticulum stress<sup>17–19</sup>.

### SIN in *S. acutum* might alleviate DPNP by regulating the IRE1 $\alpha$ -XBP1s pathway through *PTGS2*

To further screen out the effective ingredients and target genes, 14 candidate genes were imported into the STRING database for construction of the protein–protein interaction diagram (Figure 3a). Next, the data were imported into Cytoscape software to construct the protein–protein interaction network (Figure 3b,c). Furthermore, according to the order of degree value in the protein–protein interaction network from large to small, 10 key targets were obtained, which were *GRIA2*, *JUN*, *ADRA1B*, *PTGS2*, *ADRA2C*, *ADRA1A*, *ADRB2*, *PTGS1*, *NCOA2* and *RXRA* in turn (Figure 3d).

SIN is an inhibitor of *PTGS2* *in vitro* and suppresses the expression of *PTGS2*<sup>20,21</sup>. Inhibition of *PTGS2* can relieve peripheral neuropathic pain in rats<sup>22</sup>. Therefore, SIN was

selected as a key active ingredient in *S. acutum* for analysis, and *PTGS2* was selected as the target gene.

It has been documented that the activation of IRE1 $\alpha$ -XBP1s pathway can promote the release of pro-inflammatory factors, and regulation of IRE1 $\alpha$ -XBP1s can relieve pain<sup>23</sup>. *PTGS2* can activate the IRE1 $\alpha$ -XBP1s pathway<sup>8</sup>. In addition, to verify that SIN alleviated DPNP by regulating IRE1 through the IRE1 $\alpha$ -XBP1s pathway, GSE95849 microarray dataset was analyzed. The results showed that *PTGS2* expression was increased in the DPNP human samples compared with the control human samples (Figure 3e).

### SIN blocked the IRE1 $\alpha$ -XBP1s pathway by downregulating *PTGS2* to relieve pain in DPNP rats

After measurement of blood glucose level and bodyweight of the rats, we identified higher blood glucose levels and lower bodyweight in DPNP rats relative to sham-operated rats. In contrast to DPNP rats, DPNP rats treated with SIN had lower blood glucose levels and higher bodyweight; whereas both of oe-*PTGS2* and SIN treatment led to an increase in blood glucose level and a reduction in bodyweight, the effect of which could be reversed by further administration of MKC8866 (Figure 4a,b). The results of pain behavior analysis (Figure 4c) showed that PWT decreased in the DPNP rats at day 3 after STZ injection. The PWL decreased at day 1 and the lowest value was achieved at day 7 after STZ injection, and maintained until the day 14 after STZ injection, suggesting that stable mechanical and thermal pain sensitivity was formed in DPNP rats. In contrast to the DPNP rats, DPNP rats treated with SIN had increased PWT and PWL; whereas both of oe-*PTGS2* and SIN treatment reduced PWT and PWL, the effect of which could be reversed by further administration of MKC8866.

As shown by ELISA (Figure 4d), the expression of TNF- $\alpha$ , IL-1 $\beta$  and IL-6 was elevated in DPNP rats, which was decreased after SIN treatment. Compared with DPNP rats treated with SIN and oe-NC, the above-mentioned inflammatory factors increased in DPNP rats treated with SIN and oe-*PTGS2*. Compared with DPNP rats treated with SIN and oe-*PTGS2*, inflammatory factors decreased in DPNP rats treated with SIN, oe-*PTGS2* and MKC8866. Immunofluorescence results (Figure 4e) showed that the microglial marker, OX42, in the spinal dorsal horn tissue was not co-expressed with the neuronal marker, NeuN, and the astrocyte marker, GFAP. Furthermore, the expression of OX42 was higher in the DPNP rats than that in the sham-operated rats, indicating higher microglial activity in the spinal cord in DPNP rats. In contrast to the DPNP rats, microglial activity of the DPNP rats treated with SIN was weakened. In contrast to the DPNP rats treated with SIN and oe-NC, microglial activity was increased in the DPNP rats treated with SIN and oe-*PTGS2*. Relative to the DPNP rats treated with SIN and oe-*PTGS2*, opposite microglial activity occurred in the DPNP rats treated with SIN, oe-*PTGS2* and MKC8866.

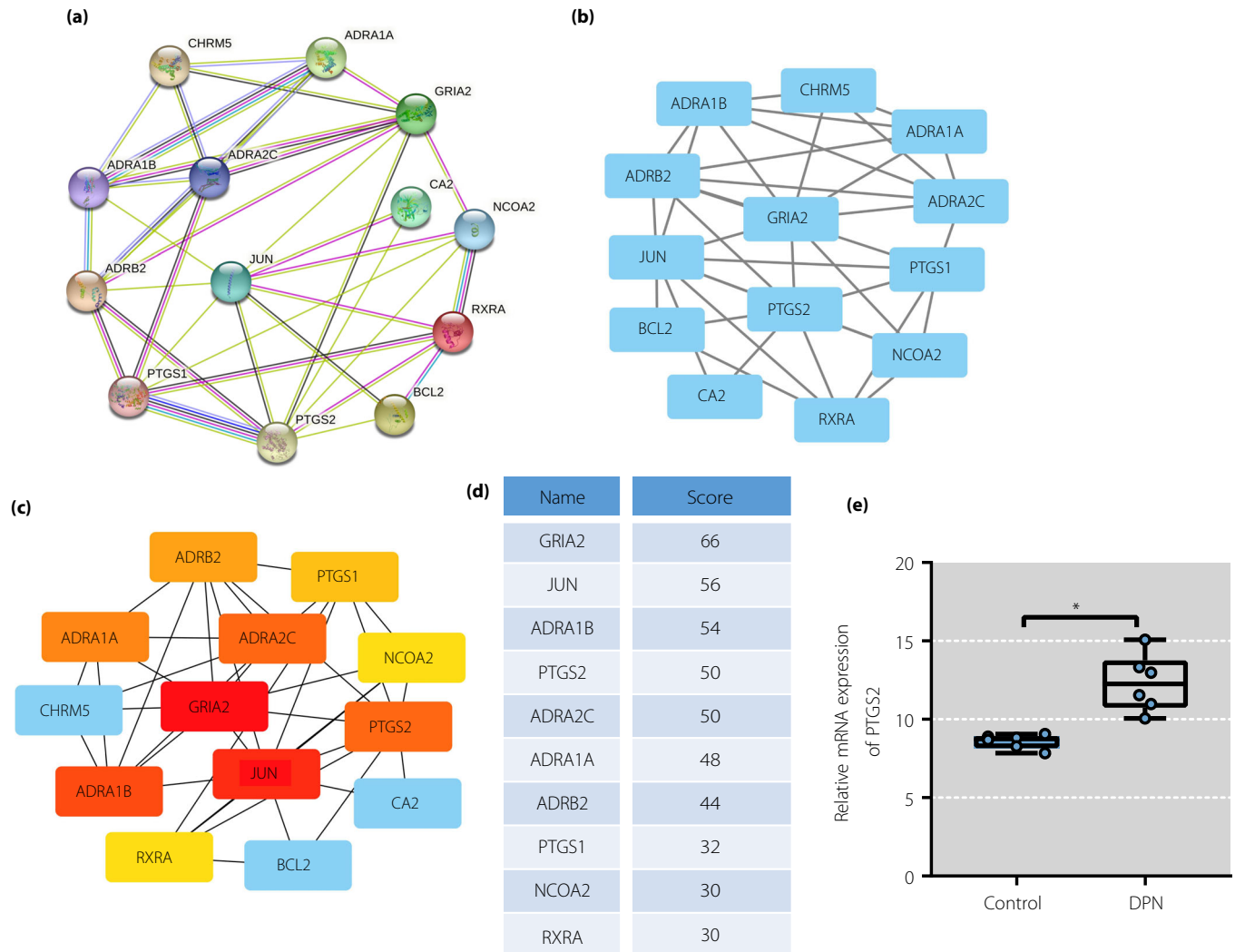


**Figure 3** | Sinomenine (SIN) in *Sinomenium acutum* might alleviate diabetic peripheral neuropathic pain by regulating inositol-requiring enzyme 1 alpha-X-box binding protein 1 pathway through prostaglandin-endoperoxide synthase 2 (*PTGS2*). (a) Protein-protein interaction network of candidate genes analyzed using String database. (b) Protein-protein interaction network constructed using Cytoscape. (c) Protein-protein interaction network of top 10 core genes screened out using Cytoscape. (d) Top 10 core genes scored using Cytoscape. (e) Bar chart of the expression of *PTGS2* in GSE95849 microarray ( $n = 6$  for the control and diabetic peripheral neuropathic pain groups, respectively). DPN, diabetic peripheral neuropathy. mRNA, messenger ribonucleic acid.

In addition, we identified elevated expression of *PTGS2*, *IRE1* and *XBPIs* in the DPNP rats, which was decreased after SIN treatment. In contrast to the DPNP rats treated with SIN and oe-NC, elevated expression of *PTGS2*, *IRE1* and *XBPIs* was witnessed in the DPNP rats treated with SIN and oe-*PTGS2*. Relative to the DPNP rats treated with SIN and oe-*PTGS2*, the expression of *PTGS2* and *IRE1* was unchanged, and the expression of *XBPIs* was reduced in the DPNP rats treated with SIN, oe-*PTGS2* and MKC8866 (Figure 4f.g). *PTGS2*-positive cells in the spinal cord of DPNP rats were detected by immunofluorescence (Figure 4h), and the results showed that *PTGS2* was mainly co-expressed with OX-42, but not with NeuN and GFAP.

### SIN inhibited the IRE1 $\alpha$ -XBP1s pathway through *PTGS2* to suppress the activation of spinal cord microglial cells and inflammatory response

Next, we isolated rat spinal cord microglial cells for further exploration. As shown by immunofluorescence, >98% of cells were OX-42-positive, showing that microglial cells with high purity were isolated from rat spinal cord (Figure 5a). *PTGS2* was overexpressed in microglial cells, validating the successful transfection (Figure 5b).

Further, microglial cell inflammatory response was stimulated with HG. After reverse transcription quantitative polymerase chain reaction and ELISA, we found that the expression of

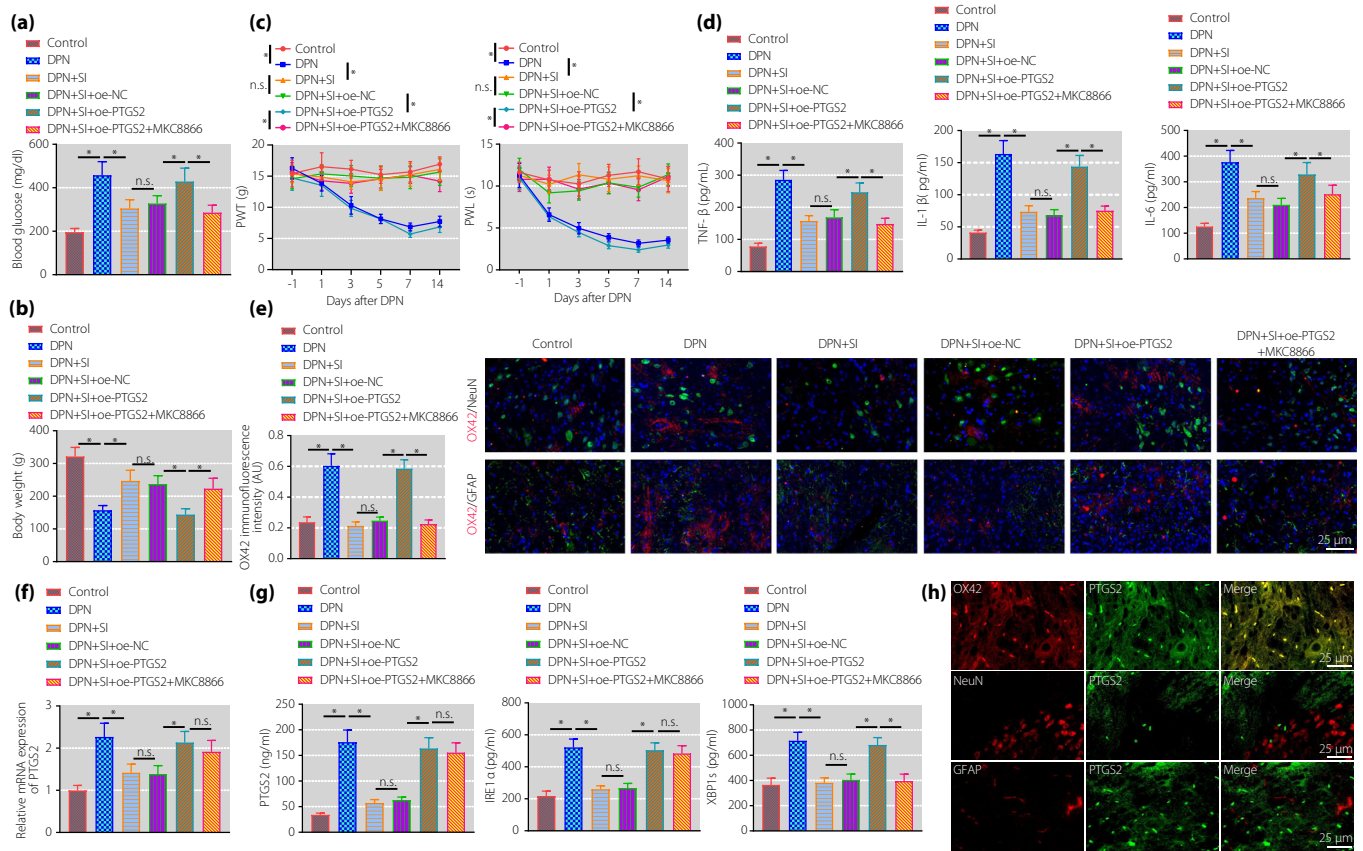


**Figure 4** | Sinomenine inhibits the inositol-requiring enzyme 1 alpha (IRE1 $\alpha$ )–X-box binding protein 1 (XBP1s) pathway activation by downregulating prostaglandin-endoperoxide synthase 2 (*PTGS2*) to relieve pain symptoms in diabetic peripheral neuropathic pain (DPNP) rats. (a) Detection of blood glucose level in DPNP rats. (b) Detection of bodyweight of DPNP rats. (c) Evaluation of the paw withdrawal threshold and paw withdrawal latency of rats before and after streptozotocin injection. (d) The expression of tumor necrosis factor- $\alpha$  (TNF- $\alpha$ ), interleukin (IL)-1 $\beta$  and IL-6 in rat spinal cord tissue measured by enzyme-linked immunosorbent assay. (e) Microglia cell activation in the spinal cord of rats measured by immunofluorescence (scale bar: 25  $\mu$ m). (f) *PTGS2* expression in the spinal cord of rats determined by quantitative reverse transcription polymerase chain reaction. (g) The expression of *PTGS2*, IRE1 $\alpha$  and XBP1s in the spinal cord of rats measured by enzyme-linked immunosorbent assay. (h) *PTGS2*-positive cells in the spinal cord of DPNP rats measured using immunofluorescence (scale bar: 25  $\mu$ m). \* $P$  < 0.05 versus the control group. n.s. indicates that the data between the two groups are not statistically significant ( $n$  = 10 in each group). DPN, diabetic peripheral neuropathy; NC, normal control; oe, overexpression; SI, sinomenine.

*PTGS2*, *IRE1* and *XBP1s* was increased in the HG-stimulated cells. In contrast to the HG-stimulated cells, the expression of the above factors was reduced in those treated with SIN. In comparison with the HG-stimulated cells treated with SIN and oe-NC, opposite results were obtained in those treated with SIN and oe-*PTGS2*. In contrast to the HG-stimulated cells treated with SIN and oe-*PTGS2*, the expression of *PTGS2* and *IRE1* was unchanged, and the expression of *XBP1s* was reduced in those treated with SIN, oe-*PTGS2* and MKC8866 (Figure 5c,d).

The expression of inflammatory factors in cell supernatant was detected by ELISA, and the results (Figure 5e) showed that the expression of TNF- $\alpha$ , IL-1 $\beta$  and IL-6 was increased in the HG-stimulated cells, which was reduced after SIN treatment. Relative to SIN + oe-NC treatment, the above expression was elevated after further treatment with oe-*PTGS2*. The trend in

response to SIN and oe-*PTGS2* in the HG-stimulated cells was reversed by co-treatment with SIN, oe-*PTGS2* and MKC8866. Immunofluorescence results (Figure 5f) showed that compared with the control cells, the expression of OX42 was increased in the HG-stimulated cells. In contrast to the HG-stimulated cells, the expression of OX42 was decreased in those treated with SIN. Relative to the HG-stimulated cells treated with SIN and oe-NC, increased OX42 expression was shown in those treated with SIN and oe-*PTGS2*, and co-treatment with SIN, oe-*PTGS2* and MKC8866 could reverse the trend.

## DISCUSSION

In the current study, we found that SIN could alleviate DPNP through regulation of *PTGS2*-mediated IRE1 $\alpha$ –XBP1s signaling pathway.

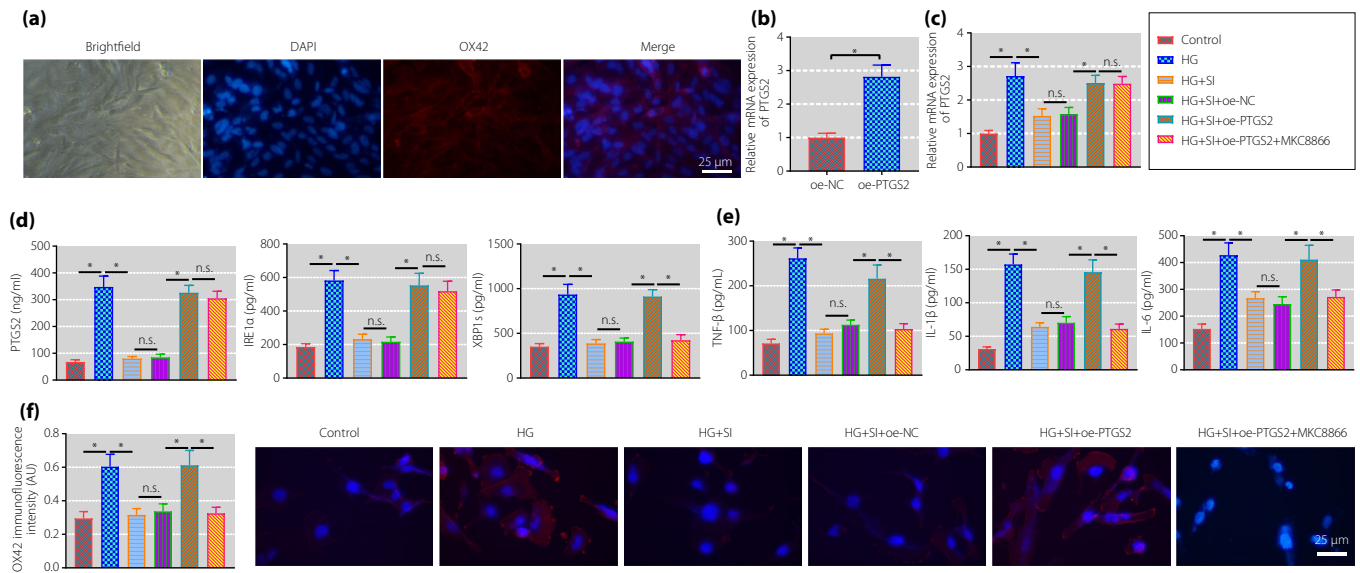


**Figure 5** | Sinomenine inhibits the inositol-requiring enzyme 1 alpha (IRE1 $\alpha$ )–X-box binding protein 1 (XBP1s) pathway through prostaglandin-endoperoxide synthase 2 (*PTGS2*) to suppress the activation of spinal cord microglia and inflammatory response. (a) The expression of OX-42 was detected by immunofluorescence to identify the purity of the isolate (scale bar: 25  $\mu$ m). (b) The transfection efficiency of *PTGS2* in spinal cord microglia measured by quantitative reverse transcription polymerase chain reaction. (c) *PTGS2* expression in rat spinal cord microglia determined by quantitative reverse transcription polymerase chain reaction. (d) The expression of *PTGS2*, IRE1 $\alpha$  and XBP1s in rat spinal cord microglia measured by enzyme-linked immunosorbent assay. (e) The expression of tumor necrosis factor- $\alpha$  (TNF- $\alpha$ ), interleukin (IL)-1 $\beta$  and IL-6 in supernatants of rat spinal cord microglia measured using enzyme-linked immunosorbent assay. (f) The activation of rat spinal cord microglia determined by immunofluorescence (scale bar: 25  $\mu$ m). \* $P$  < 0.05 versus the control group. n.s. indicates that the data between the two groups are not statistically significant. The cell experiments were repeated three times. HG, high glucose; NC, normal control; oe, overexpression; SI, sinomenine.

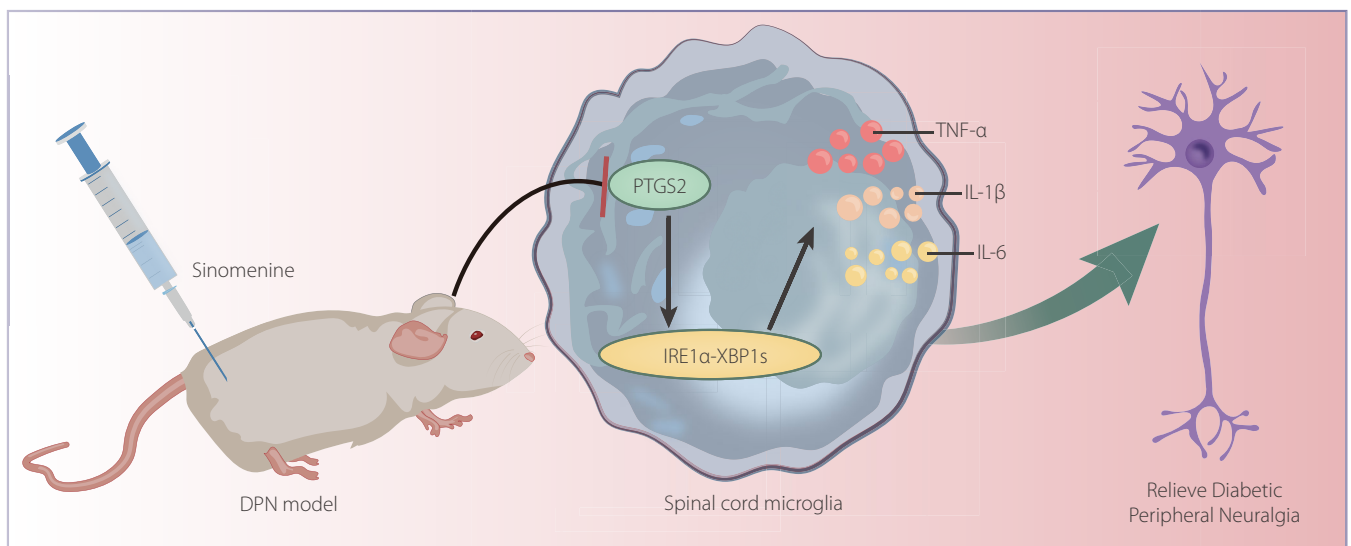


**Figure 6** | Molecular mechanism diagram of the role of sinomenine in diabetic peripheral neuropathic pain by regulating prostaglandin-endoperoxide synthase 2 (*PTGS2*)-mediated the inositol-requiring enzyme 1 alpha (IRE1 $\alpha$ )–X-box binding protein 1 (XBP1s) pathway. Sinomenine downregulates the expression of *PTGS2* to inactivate the IRE1 $\alpha$ –XBP1s signaling pathway, which inhibits microglial cell activation and the release of inflammatory factors, finally alleviating diabetic peripheral neuropathic pain. DPN, diabetic peripheral neuropathy; IL, interleukin; TNF- $\alpha$ , tumor necrosis factor- $\alpha$ .

The network pharmacological analysis combined with bioinformatics analysis carried out in the present study showed that SIN was an important active ingredient of *S. acutum* to exert efficacy on DPNP, and that *PTGS2*, the target gene of SIN, might be the key gene involved in treating DPNP. Consistent with the present results, the therapeutic effect of SIN in reducing diabetic neuropathic pain has been also previously documented<sup>24</sup>. In addition, SIN was shown to enhance the efficacy of gabapentin or ligustrazine hydrochloride in neuropathic pain in rodent animals<sup>25</sup>. Additionally, SIN could alleviate microglial mobilization and inhibit neuroinflammation to suppress experimental autoimmune encephalomyelitis<sup>26</sup>. A previous study showed that SIN can mediate anesthesia in the peripheral nervous system through modulation of voltage-gated sodium channels<sup>27</sup>. Similarly, it has also been shown that SIN might exert a modulatory effect on the TRPV signaling pathway through p38MAPK and, thus, on the peripheral nervous system response<sup>24,28,29</sup>. SIN could relieve cancer-induced bone pain partially by inhibiting microglial activation and repressing microglial JAK2/STAT3 in a rat model<sup>30</sup>. As previously reported, treatment with SIN could partially inhibit the expression of *PTGS2* to exert protective function on inflammatory pain in a rat model<sup>6</sup>. Furthermore, SIN could diminish the expression of *PTGS2* in a mouse model of osteoarthritis, resulting in repression of the inflammatory response<sup>31</sup>. Notably, the role of *PTGS2* in neuropathic pain and microglia has also been previously unveiled. Inhibition of *PTGS2* using meloxicam could play an antiallodynic role in diabetic mice with neuropathic pain, with the action site on the periphery<sup>7</sup>. In addition, highly expressed *PTGS2* could aggravate inflammatory neuronal damage induced by microglial activation<sup>32</sup>. As one recent study showed, SIN can inhibit inflammation and related pro-inflammatory factors, including IL-1 $\beta$ , IL-6 and TNF- $\alpha$ , by inhibiting NLRP3 inflammasome<sup>26</sup>, which is highly consistent with the present study.

Mechanistically, it was shown in the present study that *PTGS2* inhibited the IRE1 $\alpha$ -XBP1s signaling pathway to alleviate DPNP. Oxidative stress is one of the neuropathic factors in diabetes patients<sup>33</sup>. The linkage between oxidative stress with COX-2 has been previously documented<sup>34</sup>. Accumulating evidence has documented the interaction between *PTGS2* and IRE1 $\alpha$ -XBP1s. *PTGS2* can upregulate IRE1 $\alpha$  expression by binding to it, resulting in IRE1 $\alpha$  splicing of XBP1 messenger RNA<sup>8</sup>. Intriguingly, it was previously shown that the treatment with the *PTGS2* inhibitor, celecoxib, could contribute to a decline in the expression of IRE1<sup>35</sup>. Elevated expression of IRE1 could cause endoplasmic reticulum stress and aid in increasing paclitaxel-induced peripheral neuropathy in a rat model<sup>36</sup>. Intriguingly, the activation of IRE1 $\alpha$  and XBP1s was reported in chronic constriction injury-triggered neuropathic pain<sup>9</sup>.

In conclusion, SIN downregulates the expression of *PTGS2* to inactivate IRE1 $\alpha$ -XBP1s signaling pathway, which inhibits microglial cell activation and the release of inflammatory

factors, finally alleviating DPNP (Figure 6). Nevertheless, further study should focus on other neurological performance measurements, such as motor and/or sensory nerve conduction velocities and nerve blood flow, as well as the density of myelinated and unmyelinated nerve fibers or the intraepidermal nerve fiber density, for further validation of the present findings.

## ACKNOWLEDGMENTS

This work was supported by Excellent Youth Foundation of Hunan Provincial Department of Education (19B477), Project of Hunan Provincial Health Commission (20200018, 20200037) and Natural Science Foundation of Hunan Province (2021JJ70043).

## DISCLOSURE

The authors declare no conflict of interest.

Approval of the research protocol: This experimental procedure and animal use protocol were approved by the Animal Ethics Committee of Affiliated Huaihua Hospital, Hengyang Medical School, University of South China.

Informed consent: N/A.

Registry and the registration no. of the study/trial: 2021.09.23; HHSYY-EC-202109-K6.

Animal studies: The animal experiments followed the Animal Welfare Act and Public Health Service guidelines for the management and use of experimental animals specified by the National Institutes of Health.

## REFERENCES

1. Wei KS, Gu MZ, Zhu JW, *et al.* Current views of diabetic peripheral neuropathic pain comorbid depression – a review. *Eur Rev Med Pharmacol Sci* 2020; 24: 10663–10670.
2. Zhang B, Yu Y, Aori G, *et al.* Tanshinone IIA attenuates diabetic peripheral neuropathic pain in experimental rats via inhibiting inflammation. *Evid Based Complement Alternat Med* 2018; 2018: 2789847.
3. Toth CC, Jedrzejewski NM, Ellis CL, *et al.* Cannabinoid-mediated modulation of neuropathic pain and microglial accumulation in a model of murine type I diabetic peripheral neuropathic pain. *Mol Pain* 2010; 6: 16.
4. Huang YF, He F, Wang CJ, *et al.* Discovery of chemical markers for improving the quality and safety control of *Sinomenium acutum* stem by the simultaneous determination of multiple alkaloids using UHPLC-QQQ-MS/MS. *Sci Rep* 2020; 10: 14182.
5. Zhu Q, Sun Y, Zhu J, *et al.* Antinociceptive effects of sinomenine in a rat model of neuropathic pain. *Sci Rep* 2014; 4: 7270.
6. Yuan Y, Zhang Y, He X, *et al.* Protective effects of sinomenine on CFA-induced inflammatory pain in rats. *Med Sci Monit* 2018; 24: 2018–2024.
7. Kimura S, Kontani H. Demonstration of antiallodynic effects of the cyclooxygenase-2 inhibitor meloxicam on established

- diabetic neuropathic pain in mice. *J Pharmacol Sci* 2009; 110: 213–217.
8. Groenendyk J, Paskevicius T, Urra H, *et al.* Cyclosporine A binding to COX-2 reveals a novel signaling pathway that activates the IRE1alpha unfolded protein response sensor. *Sci Rep* 2018; 8: 16678.
  9. Gui Y, Li A, Zhang J, *et al.* alpha-Asarone alleviated chronic constriction injury-induced neuropathic pain through inhibition of spinal endoplasmic reticulum stress in an liver X receptor-dependent manner. *Anesth Analg* 2018; 127: 775–783.
  10. Lin TT, Qu J, Wang CY, *et al.* Rescue of HSP70 in spinal neurons alleviates opioids-induced hyperalgesia via the suppression of endoplasmic reticulum stress in rodents. *Front Cell Dev Biol* 2020; 8: 269.
  11. Li X, Xiang L, Lin Y, *et al.* Computational analysis illustrates the mechanism of Qingfei Paidu decoction in blocking the transition of COVID-19 patients from mild to severe stage. *Curr Gene Ther* 2022; 22: 277–289.
  12. Sheng X, Nenseth HZ, Qu S, *et al.* IRE1alpha-XBP1s pathway promotes prostate cancer by activating c-MYC signaling. *Nat Commun* 2019; 10: 323.
  13. Miao J, Zhou X, Ji T, *et al.* NF-kappaB p65-dependent transcriptional regulation of histone deacetylase 2 contributes to the chronic constriction injury-induced neuropathic pain via the microRNA-183/TXNIP/NLRP3 axis. *J Neuroinflammation* 2020; 17: 225.
  14. Yang P, He H, Xu S, *et al.* Potential molecular target prediction and docking verification of Hua-Feng-Dan in stroke based on network pharmacology. *Evid Based Complement Alternat Med* 2020; 2020: 8872593.
  15. Yang Y, Chen M, Zhai Z, *et al.* Long non-coding RNAs Gabarapl2 and Chrnb2 positively regulate inflammatory signaling in a mouse model of dry eye. *Front Med (Lausanne)* 2021; 8: 808940.
  16. Qian J, Zhao X, Wang W, *et al.* Transcriptomic study reveals recovery of impaired astrocytes contribute to neuroprotective effects of danhong injection against cerebral ischemia/reperfusion-induced injury. *Front Pharmacol* 2018; 9: 250.
  17. Zhang B, Zhang P, Tan Y, *et al.* C1q-TNF-related protein-3 attenuates pressure overload-induced cardiac hypertrophy by suppressing the p38/CREB pathway and p38-induced ER stress. *Cell Death Dis* 2019; 10: 520.
  18. Wang L, Zhang B, Huang F, *et al.* Curcumin inhibits lipolysis via suppression of ER stress in adipose tissue and prevents hepatic insulin resistance. *J Lipid Res* 2016; 57: 1243–1255.
  19. Yang F, Ma H, Butler MR, *et al.* Potential contribution of ryanodine receptor 2 upregulation to cGMP/PKG signaling-induced cone degeneration in cyclic nucleotide-gated channel deficiency. *FASEB J* 2020; 34: 6335–6350.
  20. Yang H, Yin P, Shi Z, *et al.* Sinomenine, a COX-2 inhibitor, induces cell cycle arrest and inhibits growth of human colon carcinoma cells in vitro and in vivo. *Oncol Lett* 2016; 11: 411–418.
  21. Lv Y, Li C, Li S, *et al.* Sinomenine inhibits proliferation of SGC-7901 gastric adenocarcinoma cells via suppression of cyclooxygenase-2 expression. *Oncol Lett* 2011; 2: 741–745.
  22. Stevens AM, Saleem M, Deal B, *et al.* Targeted cyclooxygenase-2 inhibiting nanomedicine results in pain-relief and differential expression of the RNA transcriptome in the dorsal root ganglia of injured male rats. *Mol Pain* 2020; 16: 1744806920943309.
  23. Chopra S, Giovanelli P, Alvarado-Vazquez PA, *et al.* IRE1alpha-XBP1 signaling in leukocytes controls prostaglandin biosynthesis and pain. *Science* 2019; 365: eaau6499.
  24. Rao S, Liu S, Zou L, *et al.* The effect of sinomenine in diabetic neuropathic pain mediated by the P2X3 receptor in dorsal root ganglia. *Purinergic Signal* 2017; 13: 227–235.
  25. Gao T, Shi T, Wiesenfeld-Hallin Z, *et al.* Sinomenine facilitates the efficacy of gabapentin or ligustrazine hydrochloride in animal models of neuropathic pain. *Eur J Pharmacol* 2019; 854: 101–108.
  26. Kiasalari Z, Afshin-Majd S, Baluchnejadmojarad T, *et al.* Sinomenine alleviates murine experimental autoimmune encephalomyelitis model of multiple sclerosis through inhibiting NLRP3 inflammasome. *J Mol Neurosci* 2021; 71: 215–224.
  27. Lee JY, Yoon SY, Won J, *et al.* Sinomenine produces peripheral analgesic effects via inhibition of voltage-gated sodium currents. *Neuroscience* 2017; 358: 28–36.
  28. Li G, Gong J, Lei H, *et al.* Promotion of behavior and neuronal function by reactive oxygen species in *C. elegans*. *Nat Commun* 2016; 7: 13234.
  29. Joksimovic SL, Jevtovic-Todorovic V, Todorovic SM. The mechanisms of plasticity of nociceptive ion channels in painful diabetic neuropathy. *Front Pain Res (Lausanne)* 2022; 3: 869735.
  30. Chen SP, Sun J, Zhou YQ, *et al.* Sinomenine attenuates cancer-induced bone pain via suppressing microglial JAK2/STAT3 and neuronal CAMKII/CREB cascades in rat models. *Mol Pain* 2018; 14: 1744806918793232.
  31. Wu Y, Lin Z, Yan Z, *et al.* Sinomenine contributes to the inhibition of the inflammatory response and the improvement of osteoarthritis in mouse-cartilage cells by acting on the Nrf2/HO-1 and NF-kappaB signaling pathways. *Int Immunopharmacol* 2019; 75: 105715.
  32. Yang L, Zhou R, Tong Y, *et al.* Neuroprotection by dihydrotestosterone in LPS-induced neuroinflammation. *Neurobiol Dis* 2020; 140: 104814.
  33. Kato A, Tatsumi Y, Yako H, *et al.* Recurrent short-term hypoglycemia and hyperglycemia induce apoptosis and oxidative stress via the ER stress response in immortalized adult mouse Schwann (IMS32) cells. *Neurosci Res* 2019; 147: 26–32.

34. Pathak SK, Sharma RA, Steward WP, *et al.* Oxidative stress and cyclooxygenase activity in prostate carcinogenesis: targets for chemopreventive strategies. *Eur J Cancer* 2005; 41: 61–70.
35. Su W, Tai Y, Tang SH, *et al.* Celecoxib attenuates hepatocyte apoptosis by inhibiting endoplasmic reticulum stress in thioacetamide-induced cirrhotic rats. *World J Gastroenterol* 2020; 26: 4094–4107.
36. Semis HS, Kandemir FM, Kaynar O, *et al.* The protective effects of hesperidin against paclitaxel-induced peripheral neuropathy in rats. *Life Sci* 2021; 287: 120104.

## SUPPORTING INFORMATION

Additional supporting information may be found online in the Supporting Information section at the end of the article.

**Table S1** | Network pharmacological analysis screens 115 effective target genes of *Sinomenium acutum*.

**Table S2** | The target proteins corresponding to the six active ingredients.

**Table S3** | The related target genes.

**Table S4** | Information about 14 intersection genes between Gene Expression Omnibus and target genes of active ingredients of *Sinomenium acutum*.